ELSEVIER

Carbohydrate Polymers 47 (2002) 59–71

Carbohydrate Polymers

www.elsevier.com/locate/carbpol

Exploring chitin morphologies in cuticle fragments of *Xiphopenaeus kroyeri* by atomic force microscopy

C.T. Andrade[a,*], K.M. Silva[a], R.A. Simão[b], C. Achete[b]

[a]*Instituto de Macromoléculas Professora Eloisa Mano, Universidade Federal do Rio de Janeiro, P.O. Box 68525, 21945-970 Rio de Janeiro, RJ, Brazil*
[b]*Programa de Engenharia Metalúrgica e de Materiais, COPPE-UFRJ, P.O. Box 68505, 21945-970 Rio de Janeiro, RJ, Brazil*

Received 25 April 2000; revised 1 November 2000; accepted 21 December 2000

Abstract

Shells of *Xiphopenaeus kroyeri*shrimp were submitted to mild acid and alkaline treatments to produce α chitin films, which were characterised by infrared spectroscopy. Dynamic AC operational mode atomic force microscopy (AFM) was used to image the external surface and regions of an inner surface of the cuticle. All samples were scanned in air. No modification of the surface structure was observed even while scanning for a long time. Chitin was visualised as microfibrils of varying thicknesses and shapes. Bundles of cracked microfibrils, as well as nearly straight microfibrils occur in the exocuticle. Scanning of an inner region clearly disclosed a bundle of microfibrils in helicoidal pattern. Non-straight microfibrils were visualised in the rostrum, as well as bundles of straight microfibrils. Estimation of the crystals thickness showed that those pertaining to bundles generally have the largest diameters.

Keywords: Atomic force microscopy; Imaging of surfaces with AFM in air; Imaging of the exocuticle of the shrimp *Xiphopenaeus kroyeri*; Imaging of stiff chitin microfibrils; Chitin

1. Introduction

Following cellulose, chitin is considered as the second most abundant biomass resource. Similarly to cellulose in plants, chitin has protective biological functions. It is present in crustacean exoskeletons and tendons, in molluscs skeletal tissue, in insect exoskeletons and in fungal cell walls (Blackwell, 1973). Chitin is a linear polysaccharide, which consists mainly of β-(1,4)-2-deoxy-2-acetamido-D-glucopyranose repeat units. *N*-deacetylated units are generally found in natural chitins, which makes these polysaccharides natural copolymers. In animal tissues, chitin occurs as highly crystalline fibrils, associated with proteins, pigments, lipids and inorganic substances, forming complex systems (Rudall & Kenchington, 1973).

Three polymorphic forms, namely α, β, and γ, have been proposed for natural chitins, to account for X-ray diffraction results (Rudall & Kenchington, 1973). α Chitin is the most abundant polymorph, whereas γ chitin is the least characterised. Although rarely found in nature, anhydrous β chitin crystallography is well established, having a monoclinic unit cell with $P2_1$ symmetry and a single chain on the 2_1-axis. Therefore, β chitin chains are packed in parallel (Blackwell, 1969; Dweltz, 1961; Gardner & Blackwell, 1975). Conversely, α chitin has a unit cell characterised by a $P2_12_12_1$ space group, which contains two antiparallel chains (Carlström, 1957; Minke & Blackwell, 1978; Saito, Okano, Chanzy & Sugiyama, 1995). The parallelism of the chains in β chitin is in agreement with unidirectional biosynthesis and concomitant crystallisation (Herth, 1979, 1980; Herth & Barthlott, 1979; Herth & Schnepf, 1982; Shillito, Lechaire & Gaill, 1993). In the case of α chitin, the mechanism of antiparallel crystallisation has not yet been established.

Electron microscopy techniques have been applied to investigate the α chitin system of the cuticle tissue of several animal orders. Nowadays, the composite model of chitin crystals embedded in a matrix of protein is fully accepted (Giraud-Guille, Chanzy & Vuong, 1990; Neville, Parry & Woodhead-Galloway, 1975; Rudall & Kenchington, 1973). Diffraction contrast transmission electron microscopy (DCTEM) was applied to image cross sections of two arthropod species. α Chitin crystals were visualised as dark units embedded in a white non-diffracting matrix (Giraud-Guille et al., 1990). By this technique, contrast depends on the orientation of the sample in relation to the electron beam (Thomas, 1986). Sharp contrast was obtained for cross

* Corresponding author. Tel.: +55-21-5627033; fax: +55-21-2701317.
E-mail address: ctandrade@ima.ufrj.br (C.T. Andrade).

0144-8617/02/$ - see front matter
PII: S0144-8617(01)00163-1

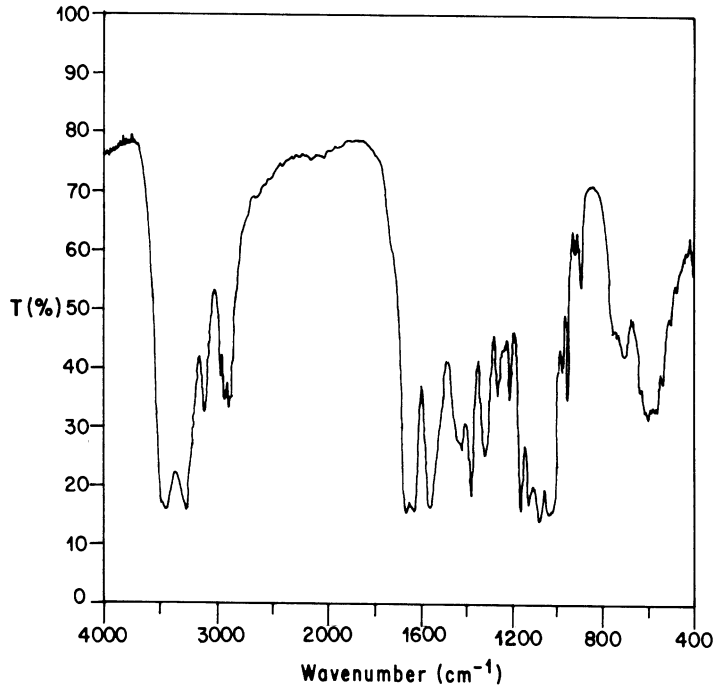

Fig. 1. Typical infrared spectrum of chitin from *X. kroyeri* cuticle (KBR disc).

sections of the cuticle principal layer of the crab *Carcinus maenas*, where chitin crystals 3 nm in width were reported to be grouped in bundles or packets with average diameter of 100 nm, each bundle containing 50–150 fibrillar crystals. These bundles would be separated by distances (Giraud-Guille et al., 1990) of 100 and 200 nm.

Atomic force microscopy (AFM) has been used with success to image the surface morphology and elucidate structure details of polymer crystals (Crämer, Fogliato Santos Lima & Magonov, 1998; Hamley, Wallwork, Smith, Fairclough, Ryan & Mai et al., 1998; Snétivy & Vancso, 1994;) and phase separated macromolecular systems (van der Berg, de Groot, van Dijk & Denley, 1994). The application of AFM to studies of soft biomaterials, particularly polysaccharides, has attracted the interest of several research groups. AFM was used to characterise the surface morphology and to measure the surface topography of hydroxypropyl cellulose thin films (Patnaik, Bunning & Wade Adams, 1995). In contact AFM mode, individual molecules and gel networks have been imaged under a nonsolvent (Gunning, Morris, Al-Assaf & Phillips, 1996; Kirby, Gunning & Morris, 1995a; Kirby, Gunning, Morris & Ridout, 1995b; Kirby, Gunning & Morris, 1996). Dynamic AFM modes, such as the tapping and the noncontact modes, have been used to characterise scleroglucan strands (Vuppu, Garcia & Vernia, 1997) and to image individual biopolymers and their supramolecular assemblies (McIntire & Brant, 1997).

In the present work, *Xiphopenaeus kroyeri* shells were demineralised and deproteinised to give chitin films, characterised by FT-IR spectroscopy. AFM in the dynamic AC operational mode was used to image the external and inner surfaces of these films with the aim of observing chitin fibrillar crystals and analysing their general features.

2. Experimental

2.1. Materials

Shells from adult shrimp *X. kroyeri* shrimp were demineralised by treatment in 0.6N HCl for 24 h. After neutralization, deproteinisation was carried out at 95°C in 1.25N NaOH for 2 h. The material was then thoroughly washed in distilled water and dried in an oven at 50°C. Residual pigments were removed by placing the chitin films successively in ethyl alcohol and acetone baths. Final drying was achieved at 50°C to constant weight (48 h).

2.2. Density measurements

Cuticle density was determined according to the method described in the literature (Saito et al., 1995). Cuticle fragments obtained as described above were immersed in xylene. Small volumes of carbon tetrachloride were added up to the level in which the fragments remained in the middle of the vessel for at least 1 day. The density of the mixture was measured and taken as the density of the cuticle.

2.3. Infrared spectra

The infrared absorption analysis of chitin samples was

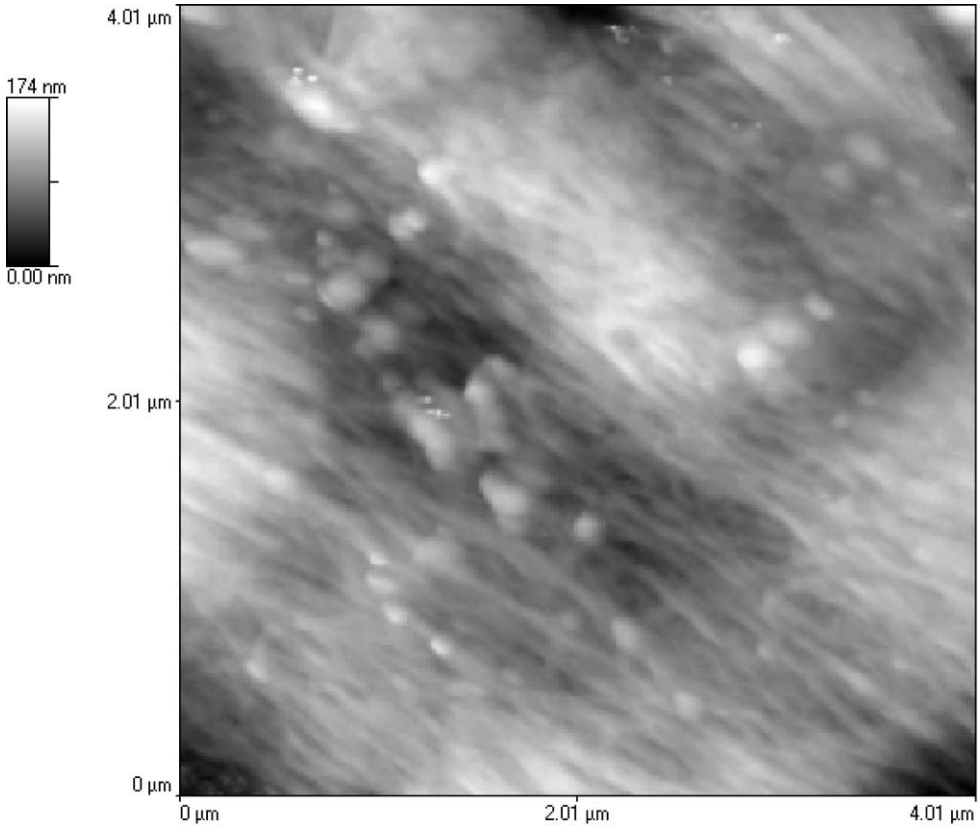

Fig. 2. AFM topographic image of the exocuticle of *X. kroyeri*.

carried out in a Perkin–Elmer 1700 FTIR in transmission mode with an accumulation of 20 scans and a resolution of 2 cm^{-1}, after being well ground and homogenised with KBr and pressed into a disc.

2.4. Atomic force microscopy

A Topometrix TMX 2010 Discoverer (Topometrix, Santa Clara, USA) instrument, equipped with a non-contact AFM probe head and a 70 µm Tripot scanner was used to obtain scanning probe microscope images. The tips (Topometrix 1660™) were made of Si, with spring constant of ca. 40 N m^{-1} and resonance frequencies in the 100–150 kHz range. Scanning was carried out at the free cantilever oscillation frequency and different amplitudes, depending on the stability and contrast obtained. The set point was fixed at 45–55% of the free oscillation amplitude. Chitin samples were fixed on double-sided adhesive tapes and the AFM images were obtained in air. Changes in the sample vertical position are presented as a height image. Changes in the phase angle of probe oscillation are presented as phase images.

3. Results and discussion

Shells of *X. kroyeri* shrimp were submitted to mild acid and alkali treatments to obtain films of unhydrolysed chitin. The infrared spectrum shown in Fig. 1 was taken from one of these samples. Three peaks can be observed in the carbonyl absorption region at around 1652, 1627 and 1558 cm^{-1}. These absorption bands, as well as that around 1420 cm^{-1}, are characteristic of α chitin (Saito, Putaux, Okano, Gaill & Chanzy, 1997). The crystallinity of the sample was evidenced by X-ray diffraction analysis. The diffractogram obtained indicates that there is a preferential orientation of the chains in the *hk*0 direction, which indicates fibrillar arrangements.

Cuticles of the shrimp *X. kroyeri* were reproductively imaged by AFM. The alkaline treatment was supposed to eliminate the epicuticle, the non-chitinous lipoprotein outer layer. Therefore, the AFM images were taken from the exocuticle, the layer that lies just beneath the epicuticle. No modification of the surface structure was observed even while scanning for a long time. Different morphological features were visualised in the scanned specimens.

Fig. 2 shows a micrometer scale AFM image that reveals the fibrillar nature of chitin. The parallel microfibrils are quite straight and aligned. Irregularly shaped nodules, probably constituted of residual resilin protein (Cutler, 1980), are visualised. Some nodules appear as very bright elements and seem to be placed on the uppermost layer. In the central part of the figure, they are placed on a dark region, which indicates the roughness of the surface.

In Fig. 3a and b, a parallel array of crystals is revealed.

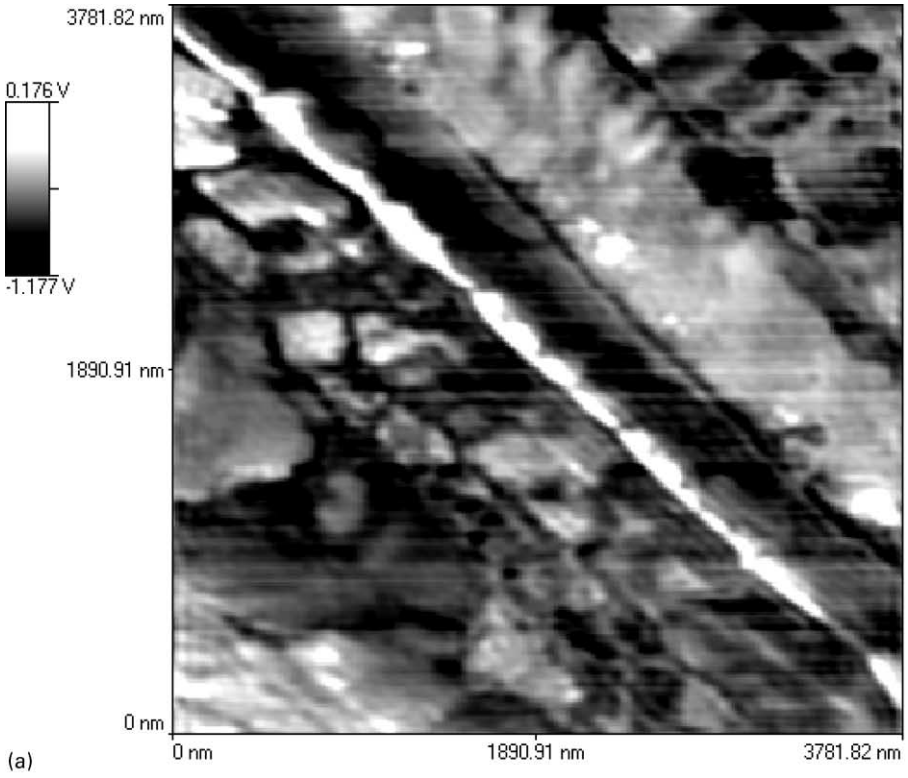

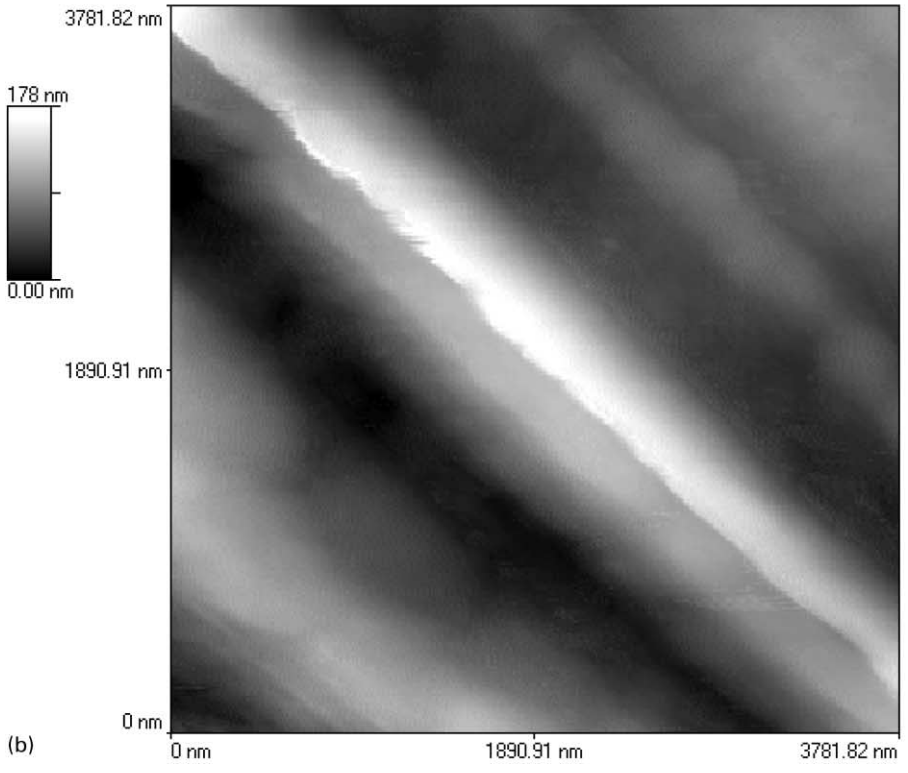

Fig. 3. AFM images of the exocuticle of *X. kroyeri*: (a) phase image; (b) topographic image.

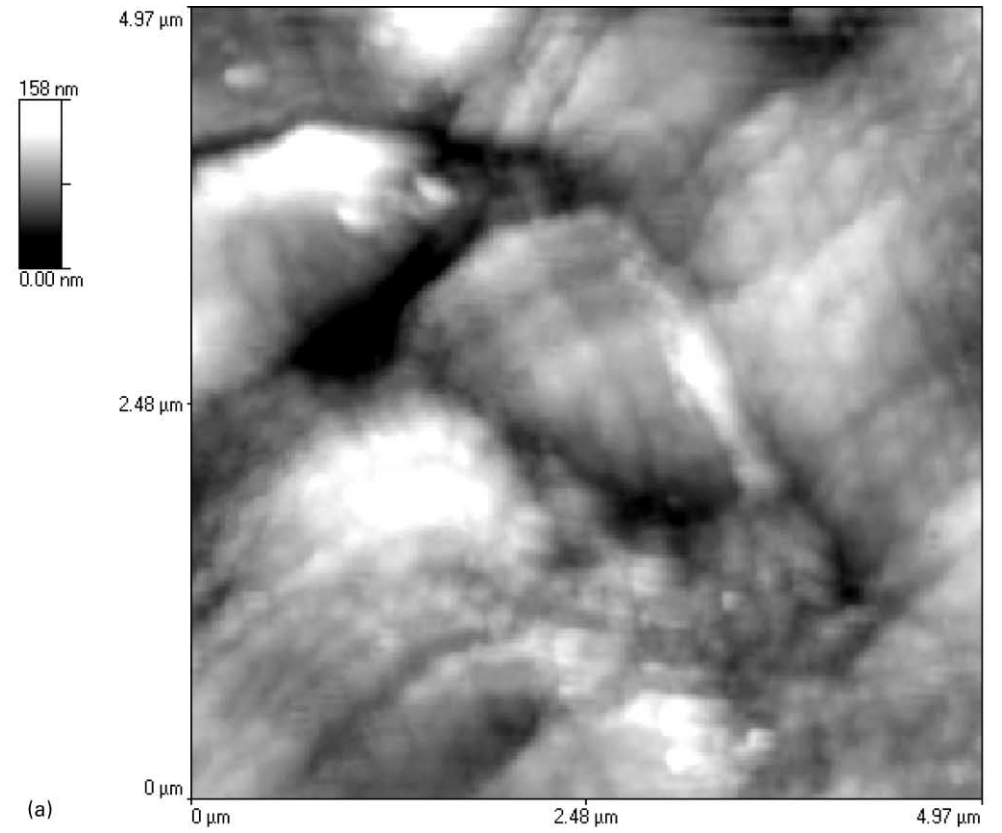

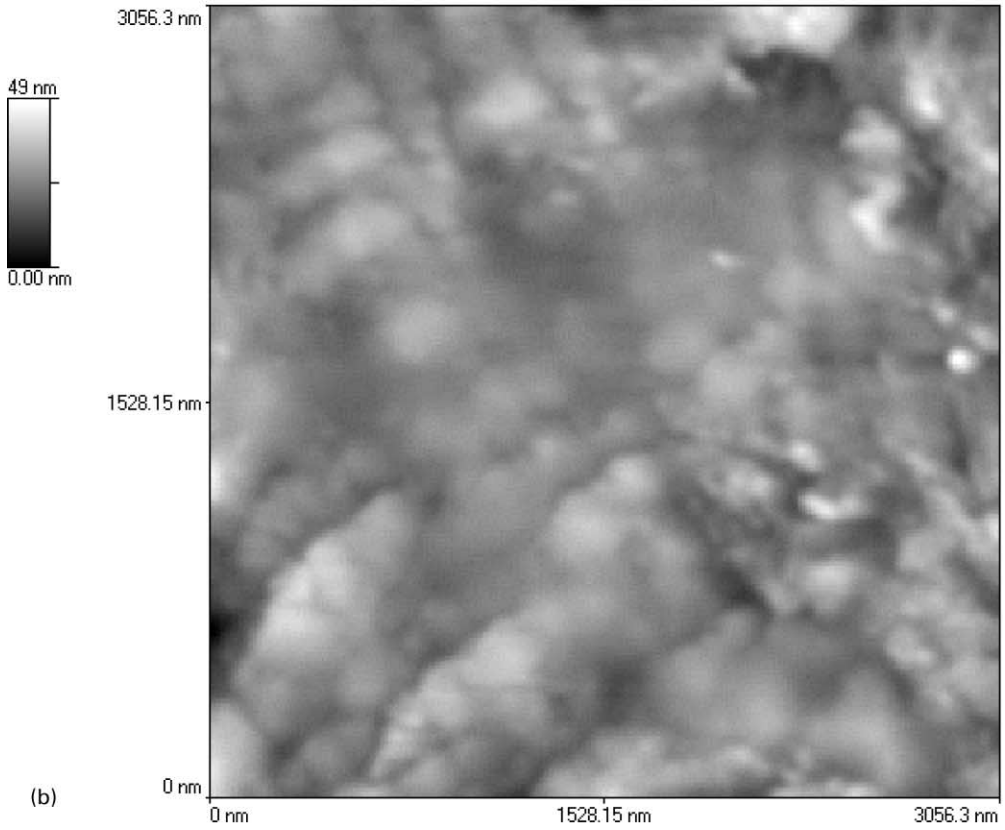

Fig. 4. AFM topographic images of the inner surface of the cuticle of *X. kroyeri*: (a) cracked crystals; (b) amplified image of cracked crystals; (c) bundle of microfibrils in helicoidal pattern; (d) a trace across the bundle estimates its thickness.

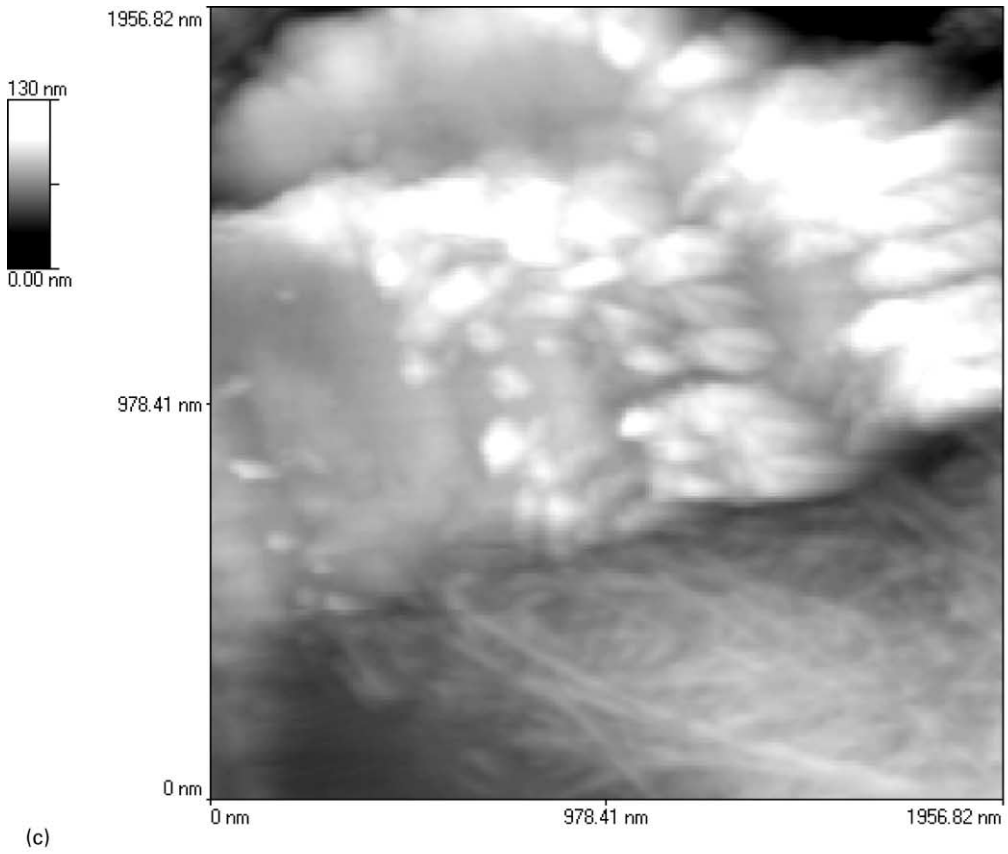

Fig. 4. (*continued*)

The thickness of the crystals varies in the range 200–500 nm. Because of their great dimensions, they can be characterised as bundles of microfibrils. In the phase image of Fig. 3a, some bundles appear irregularly cracked. In the topographic image of Fig. 3b, signs of damage are still visualised. To investigate the origin of the cracked structure, a cuticle fragment was split into thinner films and the inner surface was scanned. Fig. 4a–c show such images. In Fig. 4a, the same pattern of cracked crystals is widespread, which can be better visualised in the amplified Fig. 4b. Conversely, Fig. 4c shows an unusual image of one single bundle of microfibrils, partially fragmented. The outer crystals are cut shorter than those in the interior of the bundle, and it is not clear whether this structure is the result of a

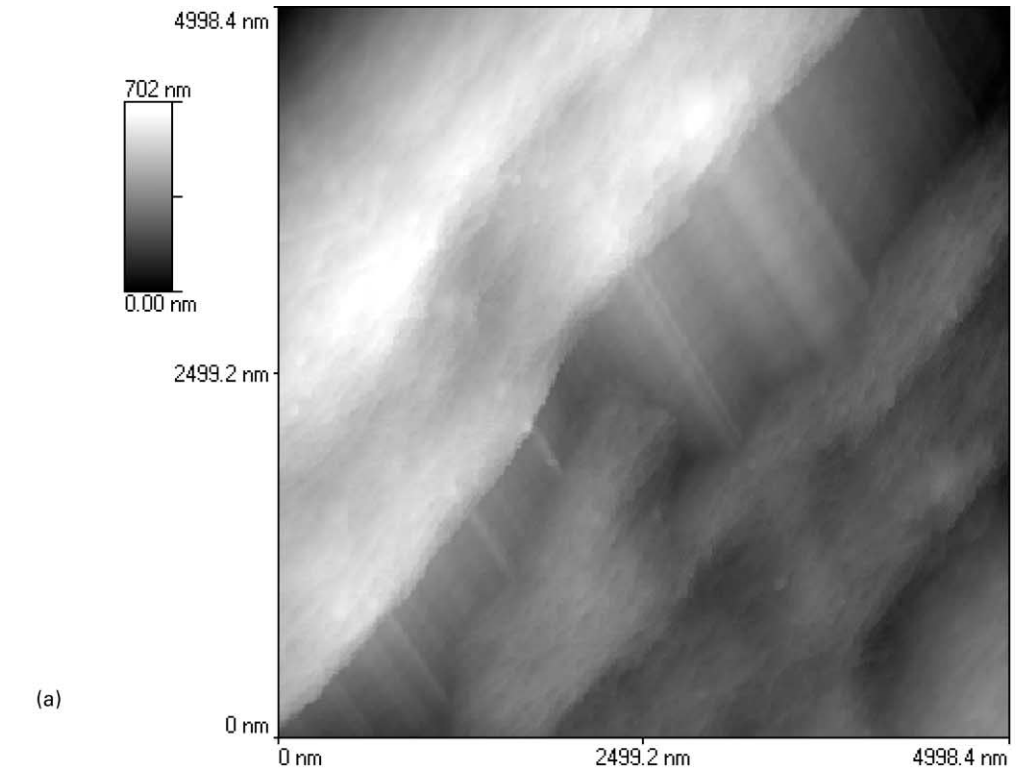

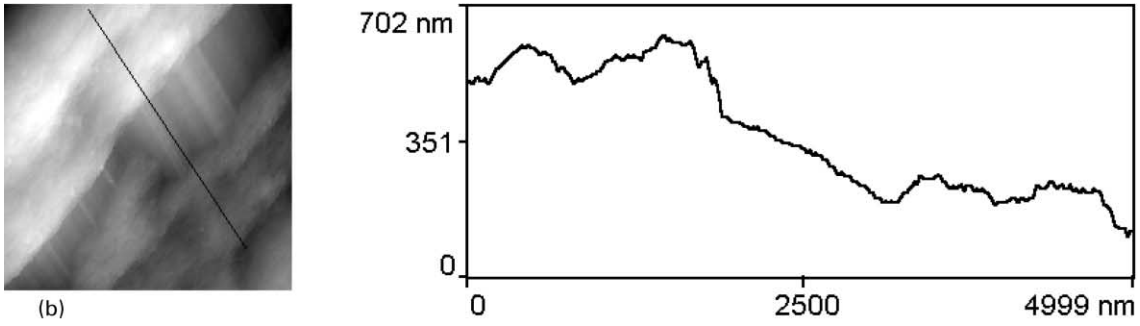

Fig. 5. AFM images of the exocuticle of *X. kroyeri*: (a) topographic image of microfibrils crystallised with imperfection; (b) a trace through irregularities showing the presence of layers; (c) topographic image of a nearby region scanned in 5a. The arrow indicates the beginning of the fissure.

natural process or the result of the mechanical force exerted by splitting. It is particularly worth mentioning the presence of microfibrils in helicoidal arrangement, despite chitin being a stiff macromolecule. At the bottom of Fig. 4c, much thinner microfibrils occur as a curled strand. A tracing (Fig. 4d) across the crystal observed in Fig. 4c was produced to estimate the thickness of the bundle, which reaches a high value of the order of 2000 nm. Although optimised, the high value should be considered with caution, since probe-broadening effects have been previously reported (Kirby et al., 1995b; McIntire & Brant, 1997).

In arthropods, the moulting process is known to occur in stages (Chapmann, 1982; Salmon & Hudson, 1997), while the cuticle remains wrapped around the animal body. Proteases and chitinases cause degradation of the old cuticle and resorption of the degradation products, which are reused

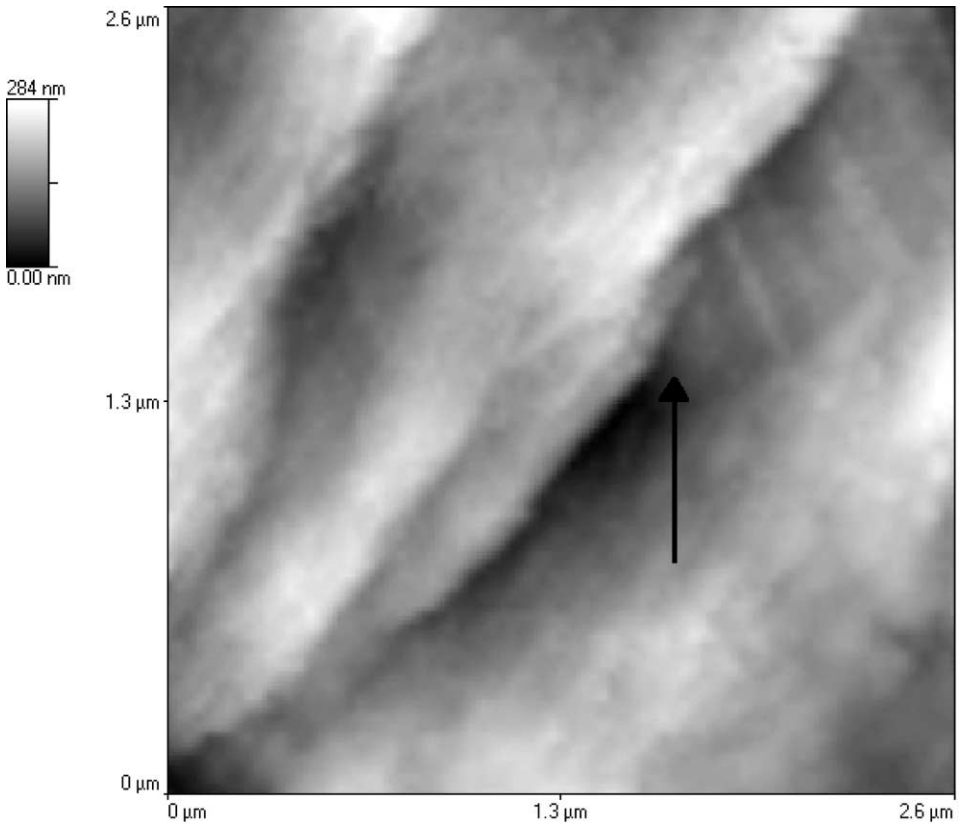

Fig. 5. (*continued*)

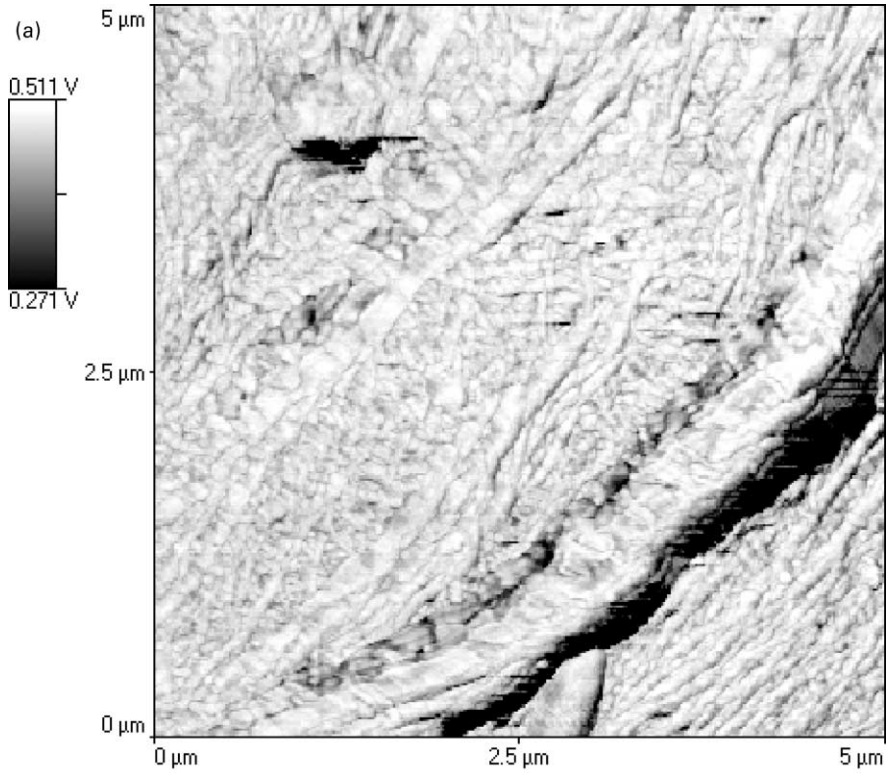

Fig. 6. AFM images of the exocuticle of *X. kroyeri* showing an interpenetrating network of microfibrils: (a) phase image; (b) topographic image; (c) a trace across the detached arced bundle.

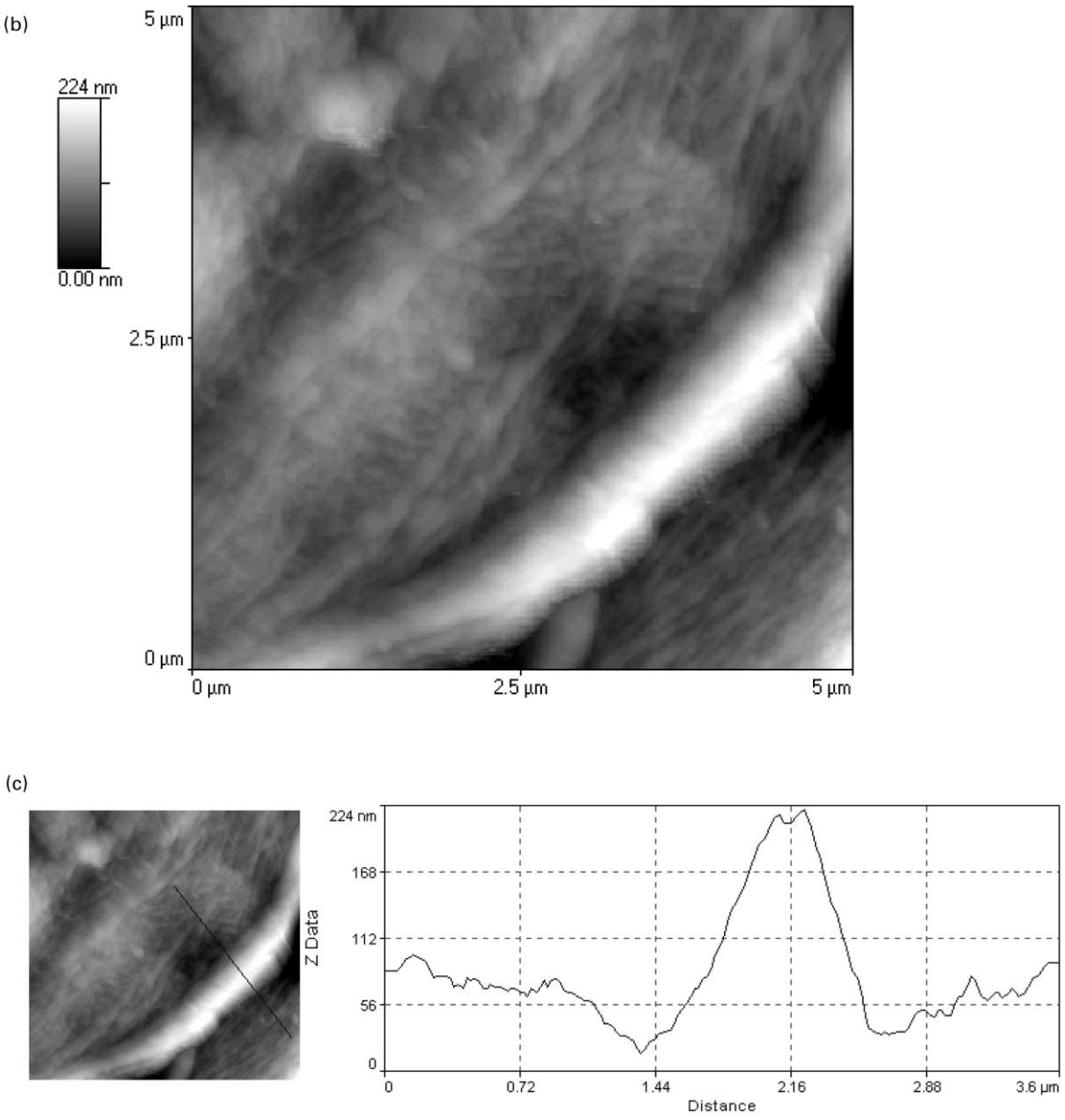

Fig. 6. (*continued*)

for the synthesis of the new cuticle (Chapmann, 1982). During moulting, the cuticle is first separated from the epidermis (apolysis), and then enzymatically degraded (ecdysis). More recently, signs of degradation have been observed by transmission electron microscopy in the principal layer of the cuticle of the crab *C. maenas* during pre-ecdysis (Compère, Thorez & Goffinet, 1998). The crack pattern imaged in Fig. 3a and b of this work may be attributed to the ecdysial stage of the exocuticle moulting process.

Figs. 5a–c show arrays of microfibrils, crystallised with some degree of imperfection. At the central part of Fig. 5a, a transversal fissure may be visualised. Throughout this fissure, an inner layer may be observed. This inner layer is constituted of parallel crystals, which are approximately perpendicular to the surface layer. A trace (Fig. 5b) across the irregular surface shows that the layers are almost parallel to each other. The topographic image shown in Fig. 5c, obtained by scanning a region nearby to that of Fig. 5a, corroborates the presence of the inner layer, since the beginning of the fissure (indicated by the arrow) is clearly visualised.

The α chitin crystals of *Sagitta* spines have a fairly constant width of about 100 nm and were observed by low-dose transmission electron microscopy as very smooth and aligned ribbon-like microfibrils (Saito et al., 1995). In the case of arthropod cuticle, much less perfect α chitin

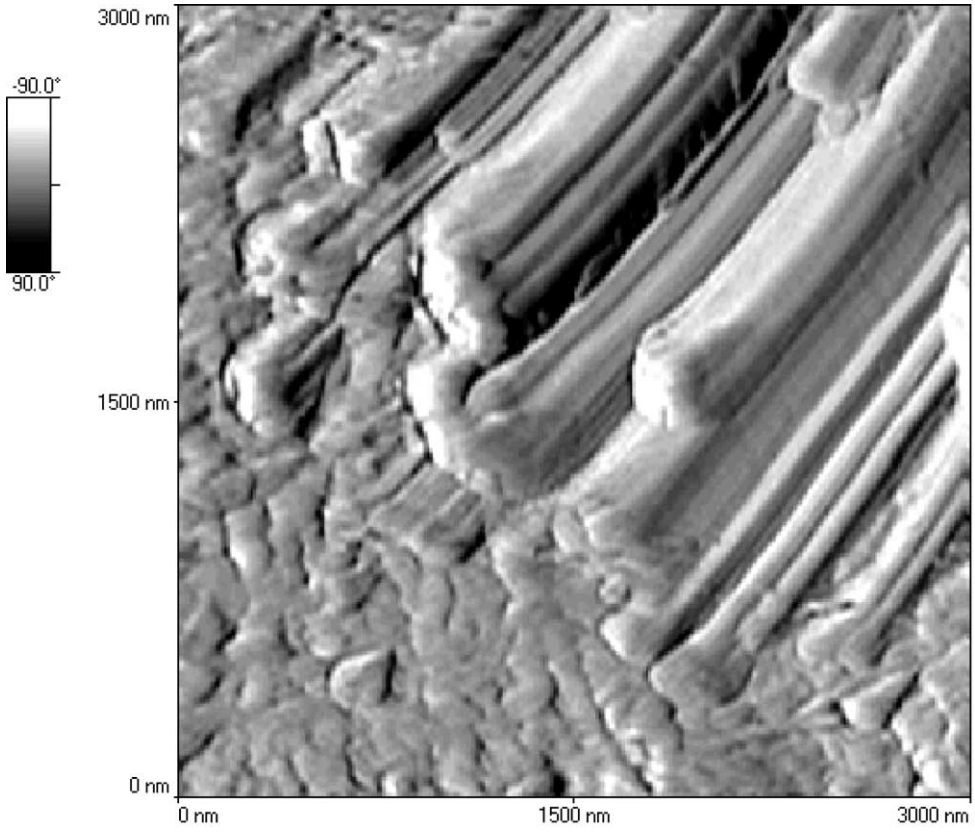

Fig. 7. AFM topographic image with shading of bundles of microfibrils found in the rostrum.

crystals were expected to occur. Nevertheless, no other microscopy technique applied to chitin systems revealed an interpenetrated network of fibrils of varying thicknesses, such as shown in Fig. 6a and b. At the bottom of these figures, an arced bundle of crystals may be visualised, which in the topographic image shown in Fig. 6b seems partially detached from the interpenetrated network on its left and from a more regular arrangement of parallel microfibrils on its right. This feature may be better visualised in Fig. 6c, in which a trace across the bottom of the scanned surface allows the observation that the bundle is more than 100 nm higher than its neighbourhood.

Fig. 7–9 show topographical images taken from the rostrum, the spinelike prolongation of the carapace. Different morphological features may be observed. In Fig. 7, nearly straight microfibrils (estimated thickness of 150–200 nm) are organised in bundles. Other images not shown in the present work also reveal the presence of such bundles in other regions of the exocuticle. Although the extremities of the microfibrils are imaged, an unequivocal characterisation may not be established in relation to their form (polygonal or round). Nevertheless, at least for the microfibrils imaged in Fig. 7, some accumulation of matter can be seen at the microfibril ends. On the right side of the figure, a bundle bears a certain similarity to the chain folding model, one of the proposed mechanisms to explain the conversion of the parallel chain arrangement to the antiparallel arrangement (Rudall, 1969).

In Fig. 8, microfibrils are in parallel alignment, in an environment of single and collapsed nodules. In this figure, as well as in Fig. 9, the microfibrils are not straight, as if they were characterised by swelling. The tracings (Fig. 8b) across some microfibrils in Fig. 8a estimate diameters in the range 40–80 nm. At the central part of Fig. 9, a non-straight and thicker microfibril may be distinguished from the others and seems to penetrate the network. Although the microfibrils of Figs. 8 and 9 have similar shape and thicknesses, the disordered morphology observed in Fig. 9 may account at least in part for the density value, $d = 1.43\ \mathrm{g\ cm^{-3}}$, determined for the cuticle fragments of *X. kroyeri*. Density values of 1.49 and 1.35 $\mathrm{g/cm^3}$ were reported for highly crystalline and amorphous chitins (Austin & Brine, 1977), respectively.

4. Conclusions

The images obtained for demineralised and deproteinised cuticle of *X. kroyeri* have proved that the AFM technique is a valuable tool for the investigation of certain biological surfaces. The images show chitin crystals of varying thicknesses. Microfibrils occur aligned in layers, which apparently display “plywood”

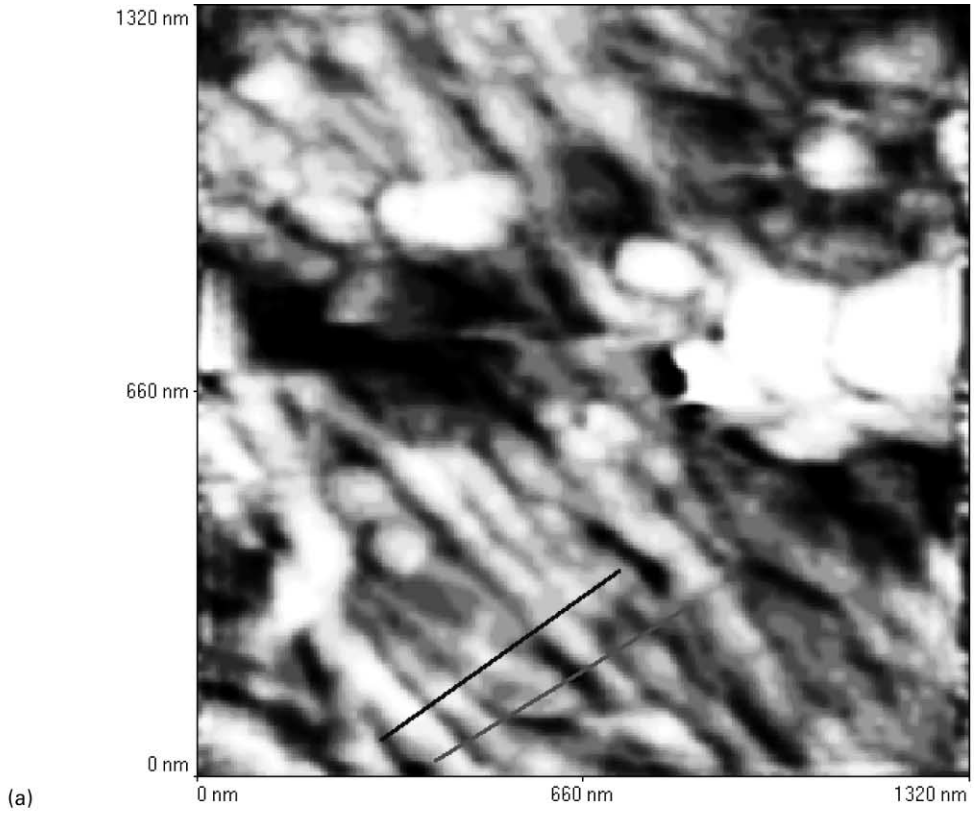

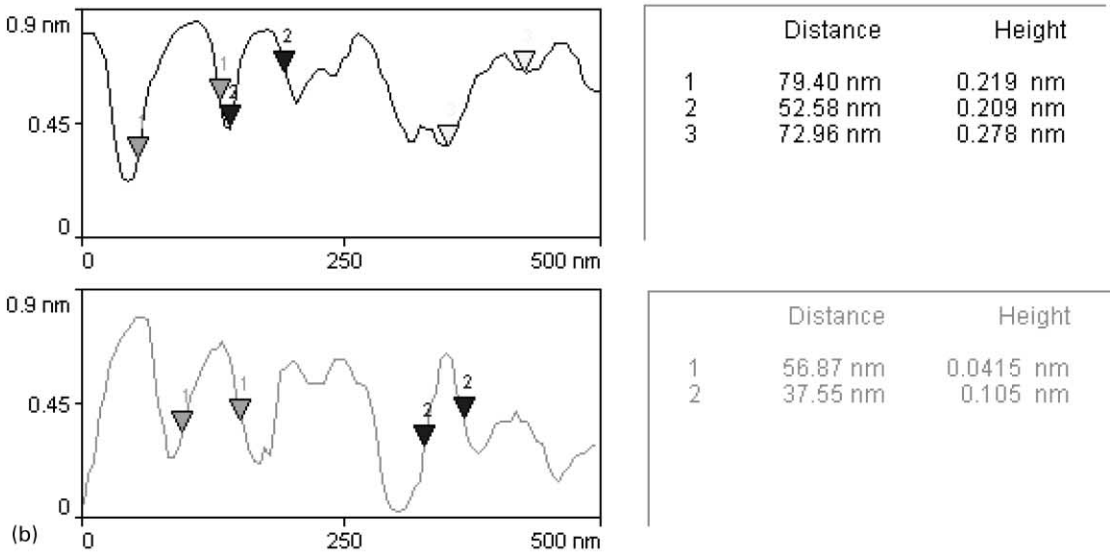

Fig. 8. (a) AFM topographic image of aligned and non-straight microfibrils found in the rostrum. (b) The trace across different regions estimate microfibrils thicknesses.

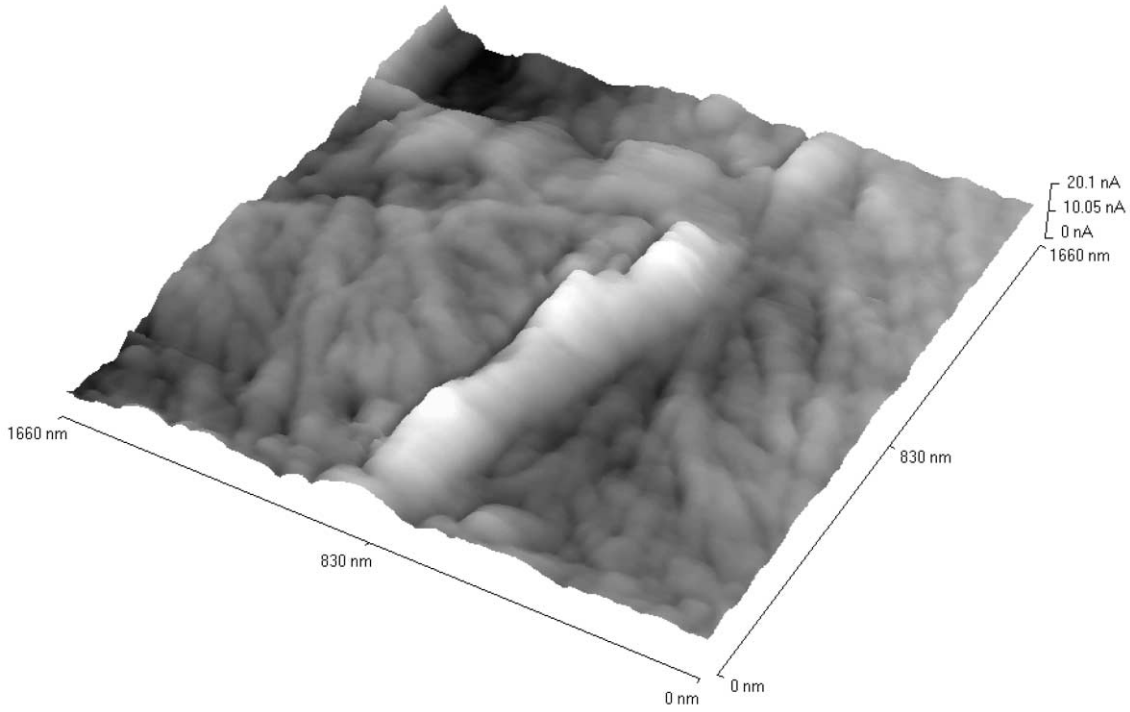

Fig. 9. AFM tridimensional topographic image of non-straight and non-aligned microfibrils found in the rostrum.

arrangements. They are also observed in interpenetrated networks and as curled strands. Bundles of microfibrils may be constituted of nearly straight microfibrils or of microfibrils in helicoidal pattern, which may reach the estimated thickness of 2000 nm. Some bundles seem to be cracked, probably as the result of the ecdysial stage of the exocuticle moulting process. Scanning of the rostrum revealed bundles of microfibrils, in which accumulation of matter could be visualised at the ends.

Acknowledgements

The authors acknowledge CNPq and PRONEX grant No. 41.96.090900 for finacial support.

References

Austin, P. R. & Brine, C. J. (1977). US Patent 4,029,727.
van der Berg, R., de Groot, H., van Dijk, M. A., & Denley, D. R. (1994). *Polymer*, *35*, 5778–5781.
Blackwell, J. (1969). *Biopolymers*, *7*, 281–298.
Blackwell, J. (1973). The polysaccharides. In A. G. Walton & J. Blackwell, *Biopolymers* (pp. 464–513). New York: Academic Press.
Carlström, D. (1957). *Journal of Biophysics and Biochemical Cytology*, *3*, 669–683.
Chapmann, R. F. (1982). *The insects: structure and function*, . (3rd ed.)Cambridge: Harvard University Press.
Compère, P., Thorez, A., & Goffinet, G. (1998). *Tissue Cell*, *30*, 41–56.
Crämer, K., Fogliato Santos Lima, M., Magonov, S. N., Hellmann, E. H., Jacobs, M., & Hellmann, G. P. (1998). *Journal of Materials Science*, *33*, 2305–2312.
Cutler, B. (1980). *Experientia*, *36*, 953–953.
Dweltz, N. E. (1961). *Biochemical and Biophysics Acta*, *51*, 283–294.
Gardner, K. H., & Blackwell, J. (1975). *Biopolymers*, *14*, 1581–1595.
Giraud-Guille, M. -M., Chanzy, H., & Vuong, R. (1990). *Journal of Structural Biology*, *103*, 232–240.
Gunning, A. P., Morris, V. J., Al-Assaf, S., & Phillips, G. O. (1996). *Carbohydrate Polymers*, *30*, 1–8.
Hamley, I. W., Wallwork, M. L., Smith, D. A., Fairclough, J. P. A., Ryan, A. J., Mai, S. -M., Yang, Y. -W., & Booth, C. (1998). *Polymer*, *39*, 3321–3326.
Herth, W. (1979). *Journal of Ultrastructural Research*, *68*, 16–27.
Herth, W. (1980). *Journal of Cell Biology*, *87*, 442–450.
Herth, W., & Barthlott, W. (1979). *Journal of Ultrastructural Research*, *68*, 6–15.
Herth, W., & Schnepf, E. (1982). Chitin-fibril formation in algae. In R. M. Brown Jr., *Cellulose and other natural polymer systems: biogenesis, structure, and degradation* (pp. 185–206). New York: Plenum Press.
Kirby, A. R., Gunning, A. P., & Morris, V. J. (1995a). *Carbohydrate Research*, *267*, 161–166.
Kirby, A. R., Gunning, A. P., Morris, V. J., & Ridout, M. J. (1995b). *Biophysics Journal*, *68*, 360–363.
Kirby, A. R., Gunning, A. P., & Morris, V. J. (1996). *Biopolymers*, *38*, 355–366.
McIntire, T. M., & Brant, D. A. (1997). *Biopolymers*, *42*, 133–146.
Minke, R., & Blackwell, J. (1978). *Journal of Molecular Biology*, *120*, 167–181.
Neville, A. C., Parry, D. A. D., & Woodhead-Galloway, J. (1975). *Journal of Cell Science*, *21*, 73–82.
Patnaik, S. S., Bunning, T. J., & Wade Adams, W. (1995). *Macromolecules*, *28*, 393–395.
Rudall, K. M. (1969). *Journal of Polymers Science Part C: Polymers Symposium*, *28*, 83–102.

Rudall, K. M., & Kenchington, W. (1973). *Biological Reviews*, *49*, 597–636.

Saito, Y., Okano, T., Chanzy, H., & Sugiyama, J. (1995). *Journal Structural Biology*, *114*, 218–228.

Saito, Y., Putaux, J. -L., Okano, T., Gaill, F., & Chanzy, H. (1997). *Macromolecules*, *30*, 3867–3873.

Salmon, S., & Hudson, S. (1997). *Journal of Macromolecular Science, Reviews of Macromolecular Chemistry and Physics*, *C37*, 199–276.

Shillito, B., Lechaire, J. P., & Gaill, F. (1993). *Journal of Structural Biology*, *111*, 59–67.

Snétivy, D., & Vancso, G. J. (1994). *Polymer*, *35*, 461–467.

Thomas, E. L. (1986). Electron microscopy. In H. F. Mark, N. M. Bikales, C. G. Overberger & G. Menges, (2nd ed.). *Encyclopedia of polymer science and engineering* (pp. 644–687). , Vol. 5. New York: Wiley Interscience.

Vuppu, A. K., Garcia, A. A., & Vernia, C. (1997). *Biopolymers*, *42*, 89–100.